*Computers, Materials & Continua* CMC, vol.60, no.3, pp.1055-1071, 2019

# An Integrated Suture Simulation System with Deformation Constraint Under A Suture Control Strategy

**Xiaorui Zhang[1, 2, 3, *], Jiali Duan[1], Jia Liu[2] and Norman I. Badler[3]**

**Abstract:** Current research on suture simulation mainly focus on the construction of suture line, and existing suture simulation systems still need to be improved in terms of diversity, soft tissue effects, and stability. This paper presents an integrated liver suture surgery system composed of three consecutive suture circumstances, which is conducive to liver suture surgery training. The physically-based models used in this simulation are based on different mass-spring models regulated by a special constrained algorithm, which can improve the model accuracy, and stability by appropriately restraining the activity sphere of the surrounding mass nodes around the suture points. We also studied the kinematic model to update the status of suture points in real time, according to an external force exerted by the operators, which can sense synchronous force feedback in return as well. Moreover, in case that the sutured wounds tear open again, a suture control strategy is designed to ensure the stability of the whole suturing procedure. Several experiments are carried out to validate the model performance in terms of model accuracy, suture control effects, and comprehensive training effects. The experiment results show that the proposed models have realistic visual and haptic feedback, stable control on the suture, as well as good training effects as an integrated liver suture surgery system compared to other suture simulation systems which only simulate suture on a single kind of soft tissue.

**Keywords:** Mass-spring model, suture simulation, virtual surgery, suture control, constraint algorithm.

## 1 Introduction

The suture is a common yet important operation in surgery. Even one small surgery needs to involve all sorts of suture circumstances from the wound on the skin to the organ or vascular injury. Compared to traditional surgery training, virtual surgical (VS) system can quickly restore the scene when any wrong operations occur and allows surgeons to repeat practice. Additionally, surgeons can conveniently experience all kinds of suture scenes, even a whole suture surgery, through virtual surgery simulation system, which

[1] Jiangsu Engineering Center of Network Monitoring, Nanjing University of Information Science & Technology, Nanjing, 210044, China.

[2] Jiangsu Collaborative Innovation Center on Atmospheric Environment and Equipment Technology, Nanjing, 210044, China.

[3] School of Engineering and Applied Science, University of Pennsylvania, Philadelphia, 19104, USA.

[*] Corresponding Author: Xiaorui Zhang. Email: zxr365@126.com.

helps to improve the training effect of the surgical operation.

In real-world surgeries, even one small surgery usually involves various suture scenes. Therefore, for improving surgery training effects, it is necessary to build a training system which involves various suture scenes and considers real-world suture situation as much as possible. However, many suture research focused on the suture line study, or only simulating a single suture scene instead of a whole suture scene with various kinds of soft tissues. For example, Brown et al. [Brown, Latombe and Montgomery (2004)] optimized a suture model to simulate the knotting procedure and they just focused on the simulation of the suture line. Shi et al. [Shi and Payandeh (2008)] simulated the suture lines with the finite element model (FEM) and realized the suture simulation of two pieces of skin, and they only simulated a single suture scene of skin. Wang et al. [Wang, Wang, Ding et al. (2010)] presented the robot-assisted operations of suture and knot-tying in a laryngeal surgery under a confined workspace, and they only simulated suture on laryngeal. Schulman et al. [Sulaiman, Hui, Bade et al. (2013)] utilized trajectory transfer algorithm to realize the automation of suture simulation. They simplified the suture scene and only simulated two flaps of tissue like skin. Jackson et al. [Jackson, Yuan, Chow et al. (2015)] proposed an algorithm based on a Non-Uniform Rational B-Spline curve to simulate a suture line, which mainly focused on the study of the suture line and paid little attention to other factors, such as the soft tissue being sutured. To sum up, although some single suture scenes that are only based on the blood vessel, skin, or laryngeal has been studied, the integrated research on multiple suture scenes has not been conducted. From the perspective of improving suture operation ability of the surgeon, an integrated suture simulation system involving many suture scenes is more conducive to surgeon's suture training.

Besides the need to construct an integrated suture simulation environment, simulating a soft tissue deformation realistically is also required during suture simulation. The key to simulate soft tissue deformation is the construction of the physical-based model. Mass-Spring Model (MSM) and FEM are two prime physical-based models. MSM [Wang, Chu, Fu et al. (2014); Duan, Huang, Chang et al. (2016); Wu, Lv and Bao (2016)] is composed of mass nodes that are connected to each other by springs, which represent the internal elastic forces acting on particles of soft tissue. Such structure makes MSM have advantages in model construction and force feedback computation. But the MSM has limited model accuracy and stability because there are many mass nodes in it and the only constraint medium are the springs, which are more suitable to represent internal forces. The springs are not enough to prevent the mass nodes from drifting during the suturing procedure. FEM [Haouchine, Cotin, Peterlik et al. (2015); Yeung, Crouch and Pothen (2016)] can be viewed as a continuous model composed of connected volume elements. It has accurate performance during simulation, while its computational procedure is relatively complex. Such characteristics make the model hard to be utilized in suture simulation since suture operation has high requirements on computational cost and haptic response. Because the MSM has faster computational speed than FEM and can provide real-time force feedback information for operators during the suture, MSM is more appropriate to be utilized in suture simulation. As stated earlier, although these existing MSM models can simulate soft tissue deformation fast and in real time, they still need to be improved in accuracy and stability. A further study [Kim and Chentanez (2012)] finds that if appropriate constraint to the activity sphere of mass nodes is applied

to MSM, a more accurate and stable simulation effect can be achieved.

During the suture simulation, the sutured wound may tear open again under the action of the suture line. In order to prevent such phenomenon, it is necessary to effectively control the wound, which will ensure the stability of the suture simulation. Payandeh et al. [Payandeh and Shi (2010)] ran a suture simulation on the skin based on a mass-spring model. The research focused on the dehiscence phenomenon of the skin caused by suture line. However, tearing in the same place on the skin will produce many small triangular patches, which may affect the reconstruction of the skin. Choi et al. [Choi, Chan and Pang (2012)] developed a prototype of suture simulator for manual skill training. In the prototype, spring-connected boxes are used to simulate soft tissues. However, due to the lack of effective control strategy against wound dehiscence, the wound cannot completely close and there are still some small gaps around the sutured points. Therefore, developing an effective suture control strategy is of great importance for enhancing simulation stability.

In summary, the current suture simulation still has some limitations, especially in terms of the integrality of suture scenes, the accuracy of the model for soft tissue simulation, and the stability of the sutured wound, thereby resulting in a negative impact on suture training for surgery. Hence, there is the need to develop an integrated suture simulation system with high accuracy and stability to enhance the training effect of suture surgery.

To address the aforementioned limitations, this paper proposes an integrated suture simulation system for multiple surgery scenes with deformation constraint under a suture control strategy. The simulation integrates three suture scenes on the skin, liver, and hepatic vascular based on three virtual soft tissue models. The integration of three suture scenes ensures the integrality of suture operation for surgeons, which facilitates the improvement of suture training effect. In order to improve the accuracy of soft tissue deformation during the suture, we propose three accurate soft tissue models by introducing a relaxed Long Range Attachment (LRA) constraint algorithm designed by Qian et al. [Qian, Bai, Yang et al. (2015)] to three basic MSMs. The proposed three accurate soft tissue models, called Uniform Tissue Suture Model (UTSM), Volumetric Organ Suture Model (VOSM), and Tubiform Tissue Suture Model (TTSM), respectively, can accommodate three suture scenes mentioned above, considering tissue property of three different organs. A suture control strategy based on distance verification is proposed to ensure the stability of suturing procedure.

The main contributions of this work are summarized as follows:

(1) This paper proposes an integrated suture simulation system suitable for multiple surgery scenes. It involves three suture scenes on the skin, liver, and hepatic vascular based on three virtual soft tissue models. Integrating three different, yet correlative suture scenes into a whole system can ensure the successful implementation of a complete suture operation for surgeons. The three correlative suture scenes can make surgeons be more familiar with the suturing procedure in a liver suture surgery, which facilitates the improvement of suture training effect for training surgeons.

(2) The paper proposes three kinds of models based on MSM for simulating different soft tissue in three correlative suture scenes. Because the three models consider typical physical property of different tissues, like skin with uniform texture, liver with volumetric shape, and vascular with the tubular structure, they can not only accommodate

the three suture scenes, but also improve the accuracy of soft tissue deformation. A relaxed LRA constraint algorithm is introduced to the proposed three accurate soft tissue models to regulate the range of soft tissue deformation. Appropriately restraining the activity sphere of mass nodes around the suture point, the proposed algorithm can further improve the model accuracy.

(3) The paper proposes a suture control strategy based on distance verification to ensure the stability of suturing procedure. In the method, a data form is designed that can record the positions of suture points, as well as the original and current distances between suture points on both sides of a wound. The suture control strategy will regulate the wound suture according to the designed data form and prevent the sutured wound from dehiscence.

The remainder of this paper is organized as follows. Section 2 describes the construction of virtual liver surgery simulation system. Section 3 presents the experiment environment and shows the suturing process and rendering effects. Section 4 carries out several validation experiments. In the last section, a summary of our work is given and future works are discussed.

## 2 Method

Considering the limitations of current suture methods discussed above, we designed an integrated liver suture surgery system, which includes following three suture scenes: suture on the skin, suture on the liver, and suture on hepatic vascular. The integration of three suture scenes can help surgeons practice on soft tissues with different structures and get familiar with a complete suturing procedure during suture surgery, which makes suture training more effective for surgeons.

To implement a complete suture operation, the integrated suture simulation system is composed of three major components: Model construction, kinematic behavior simulation, and suture control strategy. In the model construction, soft tissue model and suture line model are first constructed. Second, in the kinematic behavior simulation, deformation and force information are calculated and transformed to the operators in real time. Last but not least, in the suture control, the whole suture operation will be supervised and the suture location of the wound is adjusted based on its current and original status.

### *2.1 Model construction*

The model construction includes suture line construction and soft tissue construction. The suture lines are simulated through several small cylinders, whose trajectory is optimized by the algorithm named Follow the Leader (FTL) [Brown, Latombe and Montgomery (2004)]. Previous works on suture lines are relatively sufficient, so this study focuses on the construction of the soft tissue model. For simulating skin, liver, and hepatic vascular, we propose three new soft tissue models based on three MSM models regulated by the LRA constraint algorithm. The new models are named as Uniform Tissue Suture Model (UTSM), Volumetric Organ Suture Model (VOSM), and Tubiform Tissue Suture Model (TTSM), respectively.

*2.1.1 Mass-spring based soft tissue models*

To establish the UTSM, VOSM, and TTSM, first of all, we select appropriate MSM based models as the basic model for soft tissue construction.

The skin is of uniform texture, and a MSM with uniform structure is suitable to simulate it. Therefore, we construct the skin model based on MSM with quadrangle topologies because the human skin has uniform biological property. The structure of the skin is shown in Fig. 1(a).

The liver is a volumetric organ and one important thing to simulate suture on a volumetric organ is to present its internal volume instead of an empty shell. We construct the liver model with multi-scale mesh model [Farhang, Foruzan and Chen (2016)], which is also a MSM based model. The multi-scale mesh model shrinks the surface volume to construct a new mesh model inside the surface. Therefore, the method can simulate the inner structure of organs through MSM with lower complexity. The structure of the skin is shown in Fig. 1(b).

Hepatic vascular is of tubiform structure, in order to characterize the tubiform structure, we construct the hepatic vascular with the multi-layer mass-spring model [Pan, Chang, Yang et al. (2014)]. The model contains multiple layers to describe tubiform tissues, which is suitable for simulating thickness of a hepatic vascular wall. The mesh structure of the hepatic vascular is shown in Fig. 1(c).

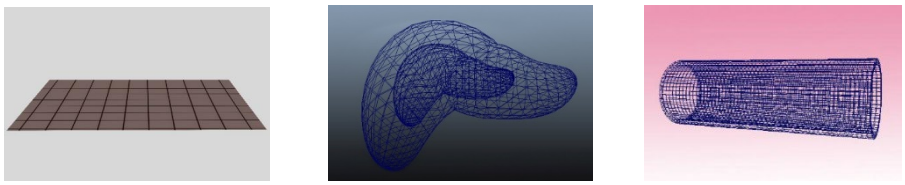

(a) skin (b) liver (c) hepatic vascular model

**Figure 1:** Structures of the three mass-spring based models

As shown in Fig. 1, skin is simulated by the MSM with quadrangle topologies. A small mesh is built inside the surface mesh of the liver to present the internal structure of liver, whose topological structure is a triangle. Hepatic vascular is constructed with multi-layer of MSM and quadrangle topology. In order to improve the model accuracy and stability, the basic models will be further regulated by the subsequent regulation process.

*2.1.2 Regulation algorithm*

As discussed before, MSM is a better choice as the basic model in this study due to its simplicity and real-time performance, but existing MSM based models cannot still well satisfy the demands of virtual suture simulation in terms of accuracy and stability. It is because springs are the only medium to connect the mass nodes, which are more suitable for force presentation. Therefore, the mass nodes cannot deform precisely without constraint besides springs. The relaxed LRA constraint algorithm designed by Qian et al. [Qian, Bai, Yang et al. (2015)] is a probable way to improve the accuracy of MSM because it can restrain the activity sphere of nodes around the attached node and ensure

the surrounding nodes move with the attached node according to their distance to the attached node. In this work, the attached node refers to the suture point.

The relaxed LRA constraint algorithm will regulate the deformation of soft tissue, according to the distance between the attached node and the surrounding nodes around the attached node. The positions of surrounding nodes $i$ will change with the positions of the attached node $j$. If a surrounding node $i$ is out of range of the initial distance $d_i^0$ between nodes $i$ and $j$, we project it to the sphere centered on the attached node $j$ with radius of $d_i$. The optimized distance $d_i$ between $i$ and $j$ can be calculated by Eq. (1).

$$d_i = d_i^0 + \beta \max((\| x_j - x_i \| - d_i^0), 0) \tag{1}$$

where $\beta$ is a relaxation parameter defined by users, which will influence the elasticity of soft tissue, $x_j$ is the positions of the attached node $j$, and $x_i$ is the position of the surrounding nodes $i$.

In order to leverage the advantage of the relaxed LRA constraint algorithm, we apply it to the three MSM based models discussed above. The regulation algorithm starts when the suture begins, which is summarized in Algorithm 1.

**Algorithm 1** The MSM regulation algorithm

Input: The position $x_j$ of the suture point $j$, and the positions $x_i$ of its surrounding nodes $i$.

for all unconstrained nodes $i$ do

apply local constraint projection to $i$ and $j$

$d_i \leftarrow d_i^0$

suture starts

for all relaxed LRA constraint do

apply constraint

apply relaxation coefficient and compute $d_{ij}$, $d_{ij} \leftarrow \beta \max((\| x_j - x_i \| - d_i), 0)$

$d_i \leftarrow d_i + d_{ij}$

Output: New position $x_j$ of the suture point $j$, and new positions $x_i$ of its surrounding nodes $i$.

The surrounding mass nodes of the suture points will move with suture points under the control of the relaxed LRA constraint algorithm. Such regulation can well regulate the deformation process of MSM, thereby ensuring its stability and accuracy in soft tissue deformation. The regulation process is illustrated in Fig. 2.

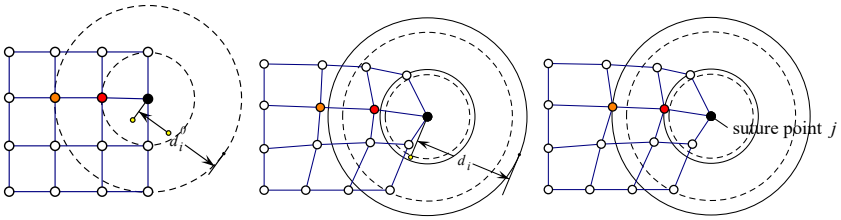


(a) Uniform Tissue Suture Model

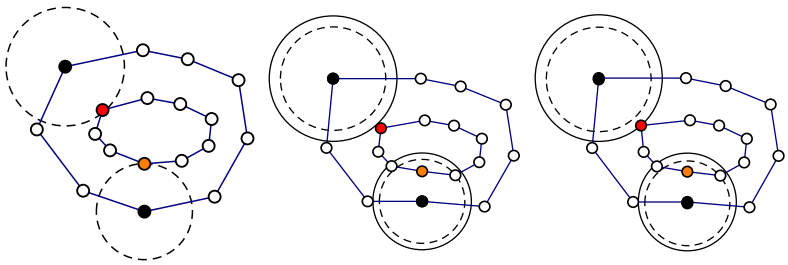

(b) Volumetric Organ Suture Model

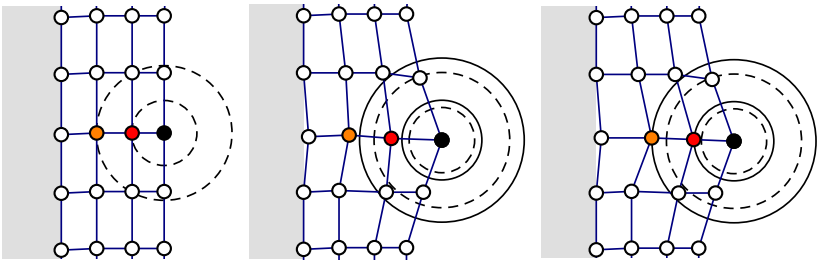

(c) Tubiform Tissue Suture Model

**Figure 2:** Regulation process of the MSMs

As is shown in Fig. 2, the blue mesh represents the soft tissues, and the black mass node represents the suture point. The white, red, and orange nodes are the surrounding nodes $i$ of the suture point. The sphere in dashed line represents the initial distance $d_i^0$, and the sphere in solid line represents the optimized distance $d_i$. Fig. 2(a) is the regulation process on the skin. In the first subfigure, the skin has not deformed. In the second subfigure, the skin starts to deform and the orange and red node move with the black node, whose move range is out of the sphere in dashed line at this time. As a result, in the third subfigure, the red and orange nodes are projected back to the sphere in a dashed line. The other white nodes also follow the above discipline. The regulation process on the surface of the liver and hepatic vascular in Figs. 2(b) and 2(c) are similar to that on the skin.

Additionally, the surface and inner layer of MSM were simultaneously sutured to simulate depth of the wound during liver suture, which can control the relationship between mass nodes of outer liver mesh and inner liver mesh, as well as better, simulate the inner structure of the liver. For the hepatic vascular suture, the proposed model can

control the deformation of the hepatic vascular wall by dealing with the relationship between different layers of the hepatic vascular wall with the regulation algorithm, which is conducive to the thickness change of the tissue wall during suture.

### *2.2 Kinematic behavior simulation*

In order to simulate the kinematic behavior of suture points and the movement of its surrounding mass nodes, we should update the position and velocity of the suture points and its surrounding nodes in real time. The positions and velocity of suture point $j$ can be updated by Eq. (2).

$$\begin{cases} v_j^{t+\Delta t} = v_j^t + a^t \cdot \Delta t \\ x_j^{t+\Delta t} = x_j^t + v_j^{t+\Delta t} \cdot \Delta t \end{cases} \tag{2}$$

where $v_j^{t+\Delta t}$ is the velocity of suture point $j$ at time $t+\Delta t$, $v_j^t$ is the velocity of suture point $j$ at time $t$, $x_j^{t+\Delta t}$ is the positions of $j$ at time $t+\Delta t$, $x_j^t$ is the positions of $j$ at time $t$, and $\Delta t$ is the update interval. In Eq. (2), $v_j^t$, $x_j^t$, and $\Delta t$ is already known. The deformation of suture points is implemented by calculating and updating the $v_j^{t+\Delta t}$ and $x_j^{t+\Delta t}$ in real time.

To obtain $v_j^{t+\Delta t}$ and $x_j^{t+\Delta t}$, we should calculate the acceleration $a^t$ of a suture point $j$ at time $t$. Therefore, we draw the kinematic sketch and carry out the following calculations. During the suture process, the suture line is always in a tensioned state. The kinematic sketch of suture line can be shown in Fig. 3.

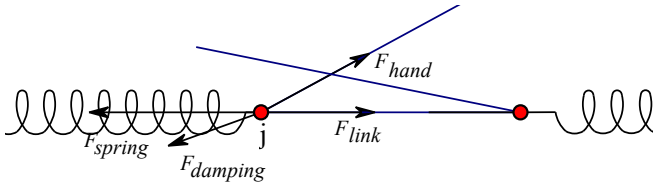


**Figure 3:** Kinematic sketch

As is shown in Fig. 3, first, we build the kinematic equation. $F_{link}$ is a force on a suture point $j$ in the direction of suture line under soft tissue, which connects the point $j$ with the suture points on the opposite side. $F_{hand}$ is a force exerted by hand on the point $j$ in the direction of suture line above soft tissue. According to physical law, $F_{link}$ and $F_{hand}$ are equal in terms of magnitude because force magnitude on the same line is identical everywhere. $F_{link}$ and $F_{hand}$ can be obtained according to the computer program and haptic interaction facility. According to Newton's third law, the magnitude of the force feedback of the system is equal to the size of $F_{hand}$, and is in the opposite direction. A kinematic equation can be built via Eq. (3).

$$\begin{cases} F_{hand} + F_{link} + F_{spring} + F_{damping} = a^t \cdot m_j \\ F_{spring} = \sum_{i \in \sigma(i)} (k \cdot (d_i - d_i^0) \cdot \dfrac{x_i - x_j}{\| x_i - x_j \|}) \\ F_{damping} = - cv_j^t \end{cases} \tag{3}$$

where $F_{spring}$ is spring tension on the suture point $j$, $F_{damping}$ is the damping force, $a$ is the acceleration of suture point $j$ and is unknown, $m_j$ is the mass of the suture point $j$ and is known, $\sigma(i)$ is set of nodes influenced by suture points, $k$ is elastic coefficient of spring, and $c$ is the damping coefficient. The equation set (3) gives the accelerated velocity $a^t$ at time $t$. The force, velocity, and acceleration in Eq. (3) are all vector quantities.

Then, we can calculate $v_j^{t+\Delta t}$ and $x_j^{t+\Delta t}$ with the acceleration $a$ of the suture point $j$, according to Eq. (2), and implement the deformation of suture points. Every time the suture points are updated, its surrounding nodes will deform with it under the regulation of the relaxed LRA constraint algorithm. The surrounding nodes of suture points will deform with it according to the relaxed LRA constraint algorithm. Meanwhile, the haptic interaction facility will feed back the force to the operators synchronously.

### *2.3 Suture control strategy*

During the suture, the sutured wound may tear open again because of dragging operations in the suture. In order to prevent such phenomenon, a suture control strategy is designed to supervise the suture process. The proposed suture control strategy is based on a data form of positions and distance of sutured points. In the data form, positions $p_{ol}^i$, $p_{cl}^i$, $p_{or}^i$, and $p_{cr}^i$ of suture points $i$, and distances $D_o^i$ and $D_c^i$ between suture points $i$ on both sides are recorded, as is shown in Tab. 1.

**Table 1:** Data form of suture control strategy

| Suture point number | left suture point | | right suture point | | Distance between suture points (mm) | |
|---|---|---|---|---|---|---|
| | Original | Current | Original | Current | Original | Current |
| $i$ | $p_{ol}^i$ | $p_{cl}^i$ | $p_{or}^i$ | $p_{cr}^i$ | $D_o^i$ | $D_c^i$ |

The strategy will judge whether the wound should be adjusted by calculating the relative error $ER_i$ of original distance $D_o^i$ and current distance $D_c^i$ between suture points on both sides. When every suture process is finished, we start the suture control strategy .The main steps are summarized in Algorithm 2.

According to Algorithm 2, the suture control strategy will supervise the suturing procedure and ensure that wound has been sutured and will not be open again. All positions of suture points on both sides and the distance between them will be recorded in the data form in real-time. The strategy will regulate the distance between all suture points until there are no more previous suture points.

**Algorithm 2** Suture control strategy

**Input:** Original positions of the suture point $i$ on both sides $p_{ol}^i$ and $p_{or}^i$, and current positions of suture points $i$ on both sides $p_{cl}^i$ and $p_{cr}^i$.

record original distance $D_o^i \leftarrow\mid p_{ol}^i - p_{or}^i \mid$

for all previous suture points do

$i \leftarrow i-1$.

record current distance $D_c^i \leftarrow\mid p_{cl}^i - p_{cr}^i \mid$

relative error $ER_i \leftarrow\mid D_c^i - D_o^i \mid / D_o^i$

if $ER_i <= 10\%$, continue

else

adjust and update $p_{cl}^i$ and $p_{cr}^i$

update current distance $D_c^i \leftarrow\mid p_{cl}^i - p_{cr}^i \mid$

$ER_i \leftarrow\mid D_c^i - D_o^i \mid / D_o^i$

**Output:** New current positions $p_{cl}^i$ and $p_{cr}^i$ of every previous suture points $i$.

## 3 Experiments and rendering

The hardware of our system is mainly composed of a desktop and a haptic device named PHANTOM OMNI. Our system runs on a desktop with an Intel Core i7 3 GHz CPU, 4.00 GB RAM, and HD7990 graphics card. The PHANTOM OMNI is a force feedback device that allows the operators to touch and operate on virtual objects. The software platform consists of VC++2015, 3DS MAX 2015, and an OPENGL graphics library. The geometric model of soft tissues is obtained from medical images and constructed in 3DS MAX 2015. The experiment environment is shown in Fig. 4.

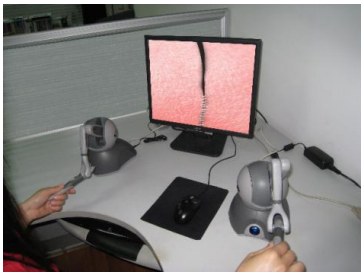

**Figure 4:** Experiment environment

During the simulation, when operators move the controller of PHANTOM OMNI, its spatial position will be detected by the position sensor in the PHANTOM OMNI. When operators contact with the soft tissue, the soft tissue deform according to the proposed algorithm. At the same time, the haptic information produced in the suture simulation system will be fed back to operators, so that the operators can feel the change of force on

the soft tissue. Several sample points will be filtered during the experiment, whose force and deformation can be output on the screen and we then record these data.

After establishing the liver suture surgery system on the experiment platform, we carried out the suture simulation for liver surgery. According to the related researches on the skin [Tai, Wei, Zhou et al. (2017)], liver [Sulaiman, Hui, Bade et al. (2013)], and hepatic vascular [Wang, Wang, Gang et al. (2016)], the parameters of UTSM, VOSM, and TTSM are set as Tab. 2.

**Table 2:** Preferences of soft tissue

| | $k$(N/mm) | $c$(Ns/m) | $\beta$ |
|---|---|---|---|
| Skin | 0.16 | 3 | 0.8 |
| Liver | 0.18 | 3 | 0.6 |
| Hepatic vascular | 0.27 | 2 | 0.4 |

(a) Suture on skin with UTSM

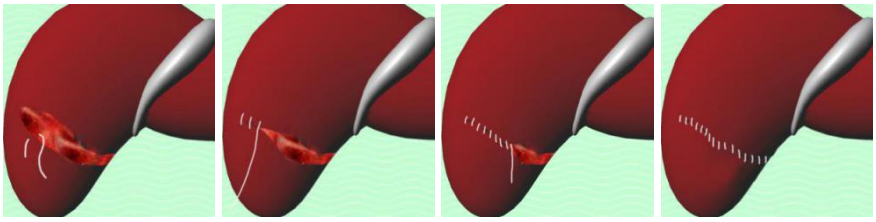

(b) Suture on liver with VOSM

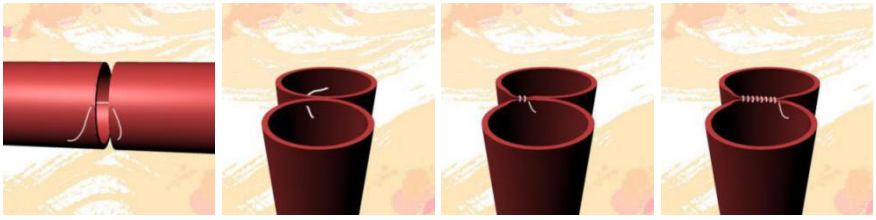

(c) Suture on hepatic vascular with TTSM

**Figure 5:** Rendering effects of suture on different soft tissue

In Tab. 2, $k$ is the elastic coefficient of springs, $c$ is the damping coefficient, and $\beta$ is the user-defined relaxation parameter. A quadrilateral mesh is utilized to simulate the skin surface and hepatic vascular wall. A triangular mesh is utilized to simulate the liver mesh. Fig. 5 shows the suture effect of the skin, liver, and hepatic vascular.

Fig. 5(a) shows that the system has vivid skin texture and elasticity, and has good deformation response. In addition, the procedure is stable and the suture line keeps tensioned during the suture. As a result, UTSM can well simulate suture on the skin. As shown in Fig. 5(b), VOSM well presents inner tissue of the liver and simulate suture on volumetric organs. The white tissue surrounding the liver is a falciform ligament, which divides the liver into left and right leaves. According to Fig. 5(c), the TTSM is aware of the thickness of the intestinal wall, and well simulates the suture on tubiform tissue.

## 4 Validation

Our suture simulation has accurate visual and haptic presentation, and can well control the wound. Also, compared to other suture simulation systems, our system can present a whole suturing procedure. In order to validate the above advantages and demonstrate our contributions, we carried out several validation experiments on the proposed suture simulation system: Model accuracy validation, suture control effect validation, and training effect validation.

### *4.1 Model accuracy validation*

Model accuracy includes deformation accuracy and haptic accuracy, which are two basic indicators of the visual and haptic model in a suture surgery system. In order to show the deformation and haptic accuracy of UTSM, VOSM, and TTSM, we compared the deformation and force data of virtual tissue simulated using a different method with the real tissue under the same external force. In this work, the deformation data refers to force-deformation curve, and the force data refers to the dist-force curve, where dist refers to the distance between sample suture points on both sides. The closer the virtual curve to the real one, the better the simulation method is. Virtual tissues are simulated with our system, and three other suture simulation systems: a skin suture system based on works of Choi et al. [Choi, Chan and Pang (2012)], a liver suture system based on works of Oshiro et al. [Oshiro and Ohkohchi (2017)], and a vessel suture system based on works of Wang et al. [Wang, Guo, Tamiya et al. (2014)].

The deformation and force data of real soft tissue from the First Affiliated Hospital of Nanjing Medical University in Nanjing are recorded as the reference substance to show the deformation accuracy of our method. We compare the force-deformation curves and dist-force curves of virtual and real skin, liver and hepatic vascular under same external forces, show the comparison results in Figs. 6 and 7.

In Fig. 6, the simulated force-deformation curves of UTSM, VOSM, and TTSM better align with the curves in the actual suture than that of other models. In Fig. 7, external force increases with the decrease of dist. It is because during the suture, as the wound is gradually closing, the resistance on the suture line continues to increase. Meanwhile, the dist-force curves of UTSM, VOSM, and TTSM better align with the curves in the actual suture than other models as well.

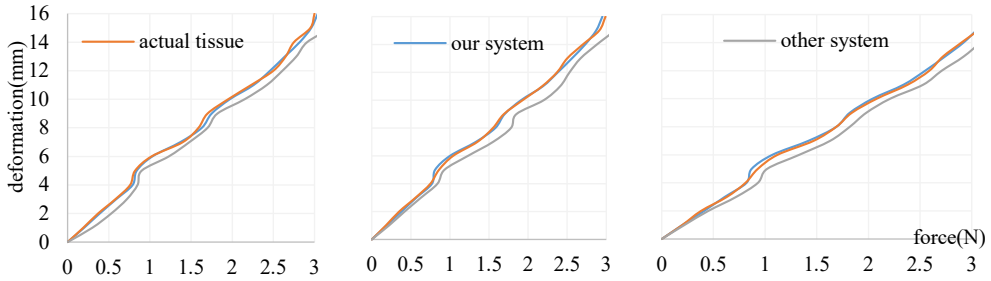


**Figure 6:** Deformation accuracy comparison

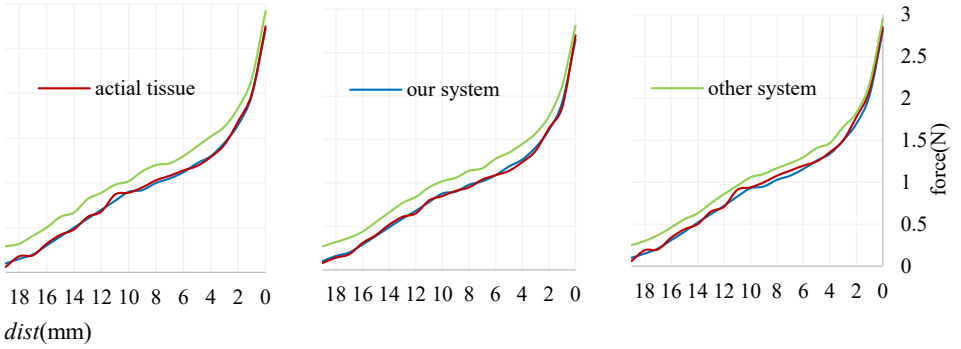


**Figure 7:** Haptic accuracy comparison

### *4.2 Validation of suture control effects*

The suture control strategy is utilized to ensure wound stability during the suturing process. In order to verify its effectiveness, when completing the skin, liver and hepatic vascular suture, we obtain the current and original distances between all suture points on both sides of the wound in the suture control strategy data table. Then, according to these data, distance radar charts of UTSM, VOSM, and TTSM are drawn as Fig. 8. A total of 12 suture points on the skin, liver and hepatic vascular are recorded, and each pair of blue and red points in the radar chart represents the current and original status of a suture point.

As shown in Fig. 8, the blue line represents the current distance between suture points, and the red line represents the original distance. In all the three figures, the blue lines and red lines basically agree with each other, indicating that there is no secondary wound dehiscence and the wound situation is stable during suture on the skin, liver, and hepatic vascular. Taking skin as an example, skin suture are completed with our system and suture system designed by Choi et al. [Choi, Chan and Pang (2012)]. The overall suture effects on skin is shown in Fig. 9.

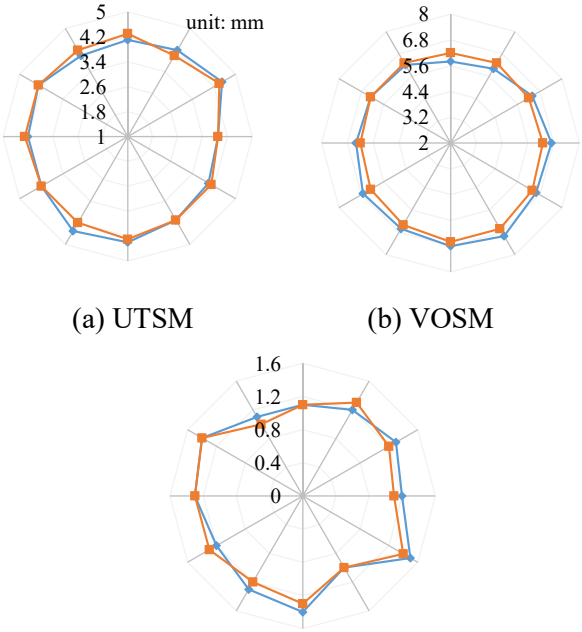


(a) UTSM (b) VOSM

(c) TTSM

**Figure 8:** Comparison of original and current distances between every suture points

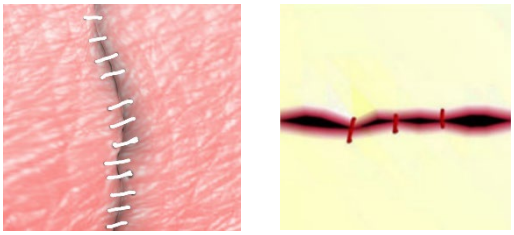

(a) Our suture system (b) Other suture system

**Figure 9:** Overall suture effects comparison on skin

As is shown in Fig. 9, the left subfigure is skin simulated with our system, and the right subfigure is the skin simulated with other systems without suture control strategy. The overall suture effect of the wound in the left subfigure is more realistic and there is no dehiscence. While the suture effect in the right subfigure is relatively stiff, and there are small gaps between every suture. The experiment results show that our suture system with suture control strategy can effectively control the wound condition.

### *4.3 Training effect validation*

To evaluate the system overall performance, 30 interns and 3 residents of the First Affiliated Hospital of Nanjing Medical University are invited. The three experts include a comprehensive surgical expert, an expert of liver surgery, and an expert of vascular surgery. The interns are arranged into two groups. The first group will carry out the suture training with our suture surgery system, and the second group will carry out the

suture training with three other suture simulation systems: a skin suture system based on works of Choi et al. [Choi, Chan and Pang (2012)], a liver suture system based on works of Oshiro et al. [Oshiro and Ohkohchi (2017)], and a vessel suture system based on works of Wang et al. [Wang, Guo, Tamiya et al. (2014)] for a comparison with our system. The training process will last for 30 minutes. Both groups will show a whole liver suture surgery before and after the training, and the residents will score them according to their performance. The experts do not know in advance which group the students belong to, and the full score is 10. Average scores of interns will be calculated after the experiment, as is shown in Tab. 3.

**Table 3:** Evaluation content of suture

| | | Before training | | After training | |
|---|---|---|---|---|---|
| | | Group 1 | Group 2 | Group 1 | Group 2 |
| Suture presentation | Skin | 6.8 | 7.4 | 9.5 | 7.2 |
| | Liver | 6.2 | 6.3 | 8.6 | 8.4 |
| | Hepatic vascular | 6.1 | 6 | 8.8 | 8.3 |
| | Total presentation | 6.5 | 6.6 | 9.2 | 7.8 |

According to Tab. 3, before training, scores of students in both groups are similar and low. After training, the average score of our system in skin suture is obviously higher than the score of the other skin suture system. The average scores of our system in the liver and hepatic vascular suture are relatively higher than scores of other suture systems as well. The comprehensive average score of our system is obviously higher than the score of the combination of the three other systems. As a result, our system can well simulate suture operation as an integrated liver suture system that's suitable for multiple suture scenes in a liver surgery.

## 5 Conclusion and future work

In this paper, we proposed an integrated suture simulation system for multiple surgery scenes with deformation constraint under a suture control strategy. In contrast to the existing suture systems based on single suture scene, the proposed integrated suture system can improve the training effect of suture surgery due to the integration of three different yet correlative suture scenes into a whole system. The results show that multiple correlative suture scenes can make surgeons be more familiar with the suturing procedure in a liver suture surgery, which facilitates the improvement of suture training effect for training surgeons. The proposed three new soft tissue deformation models based on relaxed LRA constraint algorithm can not only accommodate the three suture scenes, but also improve the accuracy of soft tissue deformation considering the typical physical property of different tissues during simulation. The kinematic model can update the status of suture points in real time, according to an external force exerted by the operators, who can synchronously receive haptic information in return with the help of haptic devices. The proposed suture control strategy based on distance verification can ensure the stability of suturing procedure.

In future works, the system can be further extended to integrate more suture scenes such as torsion or incision simulation for improving the training effect of suture surgery for surgeons. Additionally, some more sophisticated suture operations on soft tissue, such as suture needle usage can also be further studied to enrich the suture surgery system.

**Acknowledgement:** This work was supported in part by the National Nature Science Foundation of China (61502240, 61502096, 61304205, 61773219), Natural Science Foundation of Jiangsu Province (BK20141002, BK20150634).

**References:**

**Brown, J.; Latombe, J. C.; Montgomery, K.** (2004): Real-time knot-tying simulation. *Visual Computer*, vol. 20, no. 2-3, pp. 165-179.

**Choi, K. S.; Chan, S. H.; Pang, W. M.** (2012): Virtual suturing simulation based on commodity physics engine for medical learning. *Journal of Medical Systems*, vol. 36, no. 3, pp. 1781-1793.

**Duan, Y. P.; Huang, W. M.; Chang, H. B.; Chen, W. Y.; Zhou, J. Y. et al.** (2016): Volume preserved mass-spring model with novel constraints for soft tissue deformation. *IEEE Journal of Biomedical and Health Informatics*, vol. 20, no. 1, pp. 268-280.

**Farhang, S.; Foruzan, A. H.; Chen, Y. W.** (2016): A real-time stable volumetric mass-spring model based on a multi-scale mesh representation. *23rd Iranian Conference on Biomedical Engineering and 1st International Iranian Conference on Biomedical Engineering*, pp. 165-169.

**Haouchine, N.; Cotin, S.; Peterlik, I.; Dequidt, J.; Lopez, M. S. et al.** (2015): Impact of soft tissue heterogeneity on augmented reality for liver surgery. *IEEE Transactions on Visualization and Computer Graphics*, vol. 21, no. 5, pp. 584-597.

**Jackson, R. C.; Yuan, R.; Chow, D. L.; Newman, W.; Cavusoglu, M. C.** (2015): Automatic initialization and dynamic tracking of surgical suture threads. *IEEE International Conference on Robotics and Automation*, pp. 4710-4716.

**Kim, T. Y.; Chentanez, N.** (2012): Long range attachments-A method to simulate inextensible clothing in computer games. *ACM SIGGRAPH/Eurographics Symposium on Computer Animation*, pp. 305-310.

**Oshiro, Y.; Ohkohchi, N.** (2017): Three-dimensional liver surgery simulation: computer-assisted surgical planning with three-dimensional simulation software and three-dimensional printing. *Tissue Engineering Part A*, vol. 23, no. 11-12, pp. 474-480.

**Pan, J. J.; Chang, J.; Yang, X. S.; Liang, H.; Zhang, J. J. et al.** (2014): Virtual reality training and assessment in laparoscopic rectum surgery. *International Journal of Medical Robotics and Computer Assisted Surgery*, vol. 11, no. 2, pp. 194-209.

**Payandeh, S.; Shi, F.** (2010): Interactive multi-modal suturing. *Virtual Reality*, vol. 14, no. 4, pp. 241-253.

**Qian, K.; Bai, J. X.; Yang, X. S.; Pan, J. J.; Zhang, J. J.** (2015): Virtual reality based laparoscopic surgery simulation. *21st ACM Symposium on Virtual Reality Software and Technology*, pp. 69-78.

**Schulman, J.; Gupta, A.; Venkatesan, S.; Tayson-Frederick, M.; Abbeel, P.** (2013): A case study of trajectory transfer through non-rigid registration for a simplified suturing scenario. *IEEE/RSJ International Conference on Intelligent Robots and Systems*, pp. 4111-4117.

**Shi, F.; Payandeh, S.** (2008): On suturing simulation with haptic feedback. *6th International Conference on Haptics: Perception*, *Devices and Scenarios*, pp. 599-608.

**Sulaiman, S.; Hui, T. P.; Bade, A.; Lee, R.; Tanalol, S. H.** (2013): Optimizing time step size in modeling liver deformation. *IEEE 3rd International Conference on System Engineering and Technology*, pp. 209-214.

**Tai, Y. H.; Wei, L.; Zhou, H. L.; Nahavandi, S.; Shi, J. S.** (2017): Tissue and force modelling on multi-layered needle puncture for percutaneous surgery training. *IEEE International Conference on Systems, Man, and Cybernetics*, pp. 002923-002927.

**Wang, G. L.; Wang, B.; Gang, Q. G.; Zhou, S. P.; Liu, X. L.** (2016): Physical modeling of vascular tissues and stress analysis optimization based on real soft tissue characteristics. *29th International Conference on Computer Animation and Social Agents*, pp. 29-34.

**Wang, H. J.; Wang, S. X.; Ding, J. N.; Luo, H. F.** (2010): Suturing and tying knots assisted by a surgical robot system in laryngeal MIS. *Robotica*, vol. 28, no. 2, pp. 241-252.

**Wang, S. G.; Chu, L. L.; Fu, Y. L.; Gao, W. P.** (2014): An unfixed-elasticity mass spring model based simulation for soft tissue deformation. *IEEE International Conference on Mechatronics and Automation*, pp. 309-314.

**Wang, Y.; Guo, S. X.; Tamiya, T.; Hirata, H.; Ishihara, H.** (2014): A blood vessel deformation model based virtual-reality simulator for the robotic catheter operating system. *Neuroscience & Biomedical Engineering*, vol. 2, no. 3, pp. 126-131

**Wu, D.; Lv, C.; Bao, Y.** (2016): An improved vascular model based on mass spring model and parameters optimization by Gaussian processes. *IEEE International Conference on Mechatronics and Automation*, pp. 2425-2430.

**Yeung, Y. H.; Crouch, J.; Pothen, A.** (2016): Interactively cutting and constraining vertices in meshes using augmented matrices. *ACM Transactions on Graphics*, vol. 35, no. 2, pp. 1-17.